Model Studies of α-Keto Acid-Dependent Nonheme Iron Enzymes: Nitric Oxide Adducts of $[Fe^{II}(L)(O_2CCOPh)](ClO_4)$ Complexes†

Yu-Min Chiou and Lawrence Que, Jr.*

Department of Chemistry, University of Minnesota, Minneapolis, Minnesota 55455

Received March 8, 1995[⊗]

To model the putative dioxygen-bound active-site structure of α-keto acid-dependent nonheme iron enzymes, the nitrosyl adducts of iron(II)−α-keto carboxylate complexes were prepared by the treatment of $[Fe^{II}(L)(BF)]^+$ complexes with NO, where L is tris((6-methyl-2-pyridyl)methyl)amine (6TLA) or tris(2-pyridylmethyl)amine (TPA) and BF is benzoylformate. $[Fe^{II}(6TLA)(BF)](ClO_4)$ (**1**) reversibly binds NO to afford the nitrosyl adduct $[Fe(6TLA)(BF)(NO)](ClO_4)$ (**3**), while $[Fe^{II}(TPA)(BF)](ClO_4)$ (**2**) reacts with NO irreversibly to form $[Fe(TPA)(BF)(NO)](ClO_4)$ (**4**). The difference in the binding affinities of NO for **1** and **2** correlates with the higher redox potential of **1** (+870 mV vs NHE) relative to that of **2** (+340 mV) and is reflected in the ^1H NMR properties of **3** and **4**. Both nitrosyl adducts have an $\{FeNO\}^7$ configuration based on the Enemark−Feltham nomenclature and exhibit characteristic $S = {}^3/_2$ EPR signals with axial g values of 4 and 2. An X-ray diffraction study of **4** reveals a six-coordinate iron−TPA complex in which the nitrosyl ligand binds trans to the amine nitrogen and *cis* to the monodentate BF ligand. The Fe−N−O angles in the two crystallographically independent conformational isomers of **4** are 162(2) and 155(2)° with Fe−NO bond lengths of 1.70(2) and 1.74(2) Å, respectively. Crystal data are as follows: triclinic space group $P\bar{1}$; $a = 8.47(1)$ Å, $b = 11.746(8)$ Å, $c = 15.20(1)$ Å; $\alpha = 90.60(7)°$, $\beta = 99.20\ (9)°$, $\gamma = 104.30\ (7)°$; $V = 1447(5)$ Å^3; $Z = 1$; $R = 0.084$ and $R_w = 0.076$. Complexes **3** and **4** exhibit spectroscopic features comparable to those of nitrosyl adducts of several mononuclear nonheme iron proteins. Thus, the title compounds serve as models for the proposed nitrosyl (or dioxygen) adducts for the iron−cofactor complexes in α-keto acid-dependent nonheme iron enzymes.

Introduction

α-Keto acid-dependent enzymes are metalloproteins that comprise one of the largest subclasses of nonheme iron proteins with at least 12 variants.[1−3] The reaction catalyzed by these iron(II)-requiring enzymes is generalized as

$$S + O_2 + RCOCOOH \rightarrow SO + RCOOH + CO_2$$

and involves the oxidative decarboxylation of the cofactor (α-keto acid), concomitant with the oxidation of substrate. Typically, one atom from O_2 is incorporated into the resulting carboxylic acid and the other is transferred to substrate in the case of hydroxylases[4−6] or reduced to water in the case of oxidases,[7,8] simultaneous with the conversion of a C−H to a C−X bond. It is proposed that the α-keto acid cofactor coordinates to the iron(II) center and forms a ternary complex with O_2 to produce an oxidant capable of functionalizing aliphatic C−H bonds.[2]

The high-spin iron(II) state of mononuclear nonheme iron proteins is not generally spectroscopically accessible.[9,10] Nitric oxide has been effectively used as a probe of the iron(II) center, converting the usually EPR-silent $S = 2$ iron center into an EPR-active $S = {}^3/_2$ species. In the cases of isopenicillin N synthase (IPNS)[11,12] and extradiol-cleaving catechol dioxygenases such as catechol 2,3-dioxygenase (2,3-CTD) and protocatechuate 4,5-dioxygenase (4,5-PCD),[13,14] the affinity of the active site for NO increases with substrate binding. These enzyme−NO complexes serve as analogs for the possible dioxygen intermediates involved in catalysis. Such studies have allowed the identification of exogenous ligands such as substrate and solvent in the metal coordination sphere. However, NO has not previously been used as a structural or spectroscopic probe of the iron sites in α-keto acid-dependent nonheme iron enzymes.

† Abbreviations used: ACV, δ-(L-α-aminoadipoyl)-L-cysteinyl-D-valine; BF, benzoylformate; cat, catecholate dianion; 2,3-CTD, catechol 2,3-dioxygenase; deoxyHr, deoxyhemerythrin; HPTP, *N,N,N′,N′*-tetrakis(2-pyridylmethyl)-1,3-diamino-2-hydroxypropane; IPNS, isopenicillin N synthase; 6-Me-HPTP, *N,N,N′,N′*-tetrakis((6-methyl-2-pyridyl)methyl)-1,3-diamino-2-hydroxypropane; Me_3TACN, *N,N′,N″*-trimethyl-1,4,7-triazacyclononane; OBz, benzoate; PCA, protocatechuic acid; 3,4-PCD, protocatechuate 3,4-dioxygenase; 4,5-PCD, protocatechuate 4,5-dioxygenase; salen, *N,N′*-ethylenebis(salicylideneamine); SBL, soybean lipoxygenase; TMC, 1,4,8,11-tetramethyl-1,4,8,11-tetraazacyclodecane; TMPzA, tris((3,5-dimethyl-1-pyrazolyl)methyl)amine; TPA, tris(2-pyridylmethyl)amine; 6TLA, tris(6-methyl-2-pyridylmethyl)amine.

⊗ Abstract published in *Advance ACS Abstracts,* May 15, 1995.

(1) Abbott, M. T.; Udenfriend, S. In *Molecular Mechanisms of Oxygen Activation*; Hayaishi, O., Ed.; Academic Press: New York, 1974; pp 167−214.
(2) Hanauske-Abel, H. M.; Günzler, V. *J. Theor. Biol.* **1982**, *94*, 421−455.
(3) Kivirikko, K. I.; Myllylä, R.; Pihlajaniemi, T. In *Post-Translational Modifications of Proteins*; Harding, J. J., Crabbe, M. J. C., Eds.; CRC Press: Boca Raton, FL, 1992; pp 1−51.
(4) Kivirikko, K. I.; Myllylä, R.; Pihlajaniemi, T. *FASEB J.* **1989**, *3*, 1609−1617.
(5) Thornburg, L. D.; Stubbe, J. *J. Am. Chem. Soc.* **1989**, *111*, 7632−7633.
(6) Thornburg, L. D.; Lai, M.-T.; Wishnok, J. S.; Stubbe, J. *Biochemistry* **1993**, *32*, 14023−14033.
(7) Baldwin, J. E.; Adlington, R. M.; Crouch, N. P.; Schofield, C. J.; Turner, N. J.; Aplin, R. T. *Tetrahedron* **1991**, *47*, 9881−9900.
(8) Townsend, C. A.; Basak, A. *Tetrahedron* **1991**, *47*, 2591−2602.
(9) Solomon, E. I.; Zhang, Y. *Acc. Chem. Res.* **1992**, *25*, 343−352.
(10) Que, L., Jr. In *Bioinorganic Catalysis*; Reedijk, J., Ed.; Marcel Dekker: New York, 1993; pp 347−393.
(11) Chen, V. J.; Orville, A. M.; Harpel, M. R.; Frolik, C. A.; Surerus, K. K.; Münck, E.; Lipscomb, J. D. *J. Biol. Chem.* **1989**, *264*, 21677−21681.
(12) Orville, A. M.; Chen, V. J.; Kriauciunas, A.; Harpel, M. R.; Fox, B. G.; Münck, E.; Lipscomb, J. D. *Biochemistry* **1992**, *31*, 4602−4612.
(13) Arciero, D. M.; Orville, A. M.; Lipscomb, J. D. *J. Biol. Chem.* **1985**, *260*, 14035−14044.
(14) Arciero, D. M.; Lipscomb, J. D. *J. Biol. Chem.* **1986**, *261*, 2170−2178.

0020-1669/95/1334-3270$09.00/0

Table 1. Crystallographic Data for [Fe(TPA)(BF)(NO)](ClO$_4$)·0.5C$_3$H$_6$O (**4**)

formula	$C_{27.5}H_{26}ClFeN_5O_{8.5}$	fw	653.835
a, Å	8.47(1)	space group	$P\bar{1}$ (No. 1)
b, Å	11.746(8)	temp, K	176
c, Å	15.20(1)	λ, Å	0.7107
α, deg	90.60(7)	D(calc), g cm^{-3}	1.501
β, deg	99.20(9)	μ, cm^{-1}	6.70
γ, deg	104.30(7)	R^a	0.084
V, Å^3	1447(5)	$R_w{}^b$	0.076
Z	2		

$^a R = (\sum|F_o - F_c|)/(\sum F_o)$. $^b R_w = \{(\sum w|F_o - F_c|^2)/(\sum w(F_o)^2)\}^{1/2}$.

Such studies should provide information about the active-site structures of these enzymes.

As part of our synthetic modeling effort to provide fundamental structural and mechanistic information on iron−α-keto carboxylate moieties of significance to α-keto acid-dependent enzymes, we have prepared and fully characterized the first iron(II) complexes of α-keto acids, [Fe^{II}(6TLA)(BF)](ClO$_4$) (**1**) and [Fe^{II}(TPA)(BF)(MeOH)](ClO$_4$) (**2**).[15-17] We have demonstrated that the reactions of both **1** and **2** with dioxygen result in quantitative oxidative decarboxylation of the iron-bound benzoylformate with concomitant oxidation of substrates. However, the nature of the active intermediates has not yet been determined. In this study, we explore the chemistry of NO binding to both model complexes and report the structural and spectroscopic properties of these novel iron−α-keto carboxylate−nitrosyl complexes. These complexes may be considered as models for the dioxygen-bound iron−cofactor ternary complex proposed for α-keto acid-dependent iron enzymes.

Experimental Section

General Procedures. Nitric oxide (98.19%, Matheson) was passed through a 10 M KOH(aq) solution prior to use. Argon gas (commercial grade, Airgas Products Inc.) was passed through an oxygen scrubber (Chemical Dynamics Corp.) before use. All reagents and solvents were purchased from commercial sources and used as received unless noted otherwise. Preparation and handling of air-sensitive materials were carried out under an argon atmosphere using standard Schlenk techniques or in a Vacuum/Atmospheres TS-5000 anaerobic box. Deoxygenation of solvents and solutions was effected by repeated vacuum/purge cycles using argon. Elemental analyses were performed by M-H-W Laboratories, Phoenix, AZ.

Preparation of NO Complexes. [Fe^{II}(6TLA)(BF)](ClO$_4$) (**1**) and [Fe^{II}(TPA)(BF)(MeOH)](ClO$_4$) (**2**) were prepared as reported previously.[15,17] *Caution: The perchlorate salts in this study are potentially explosive and should be handled with care.*

[Fe(6TLA)(BF)(NO)](ClO$_4$) (3). Complex **1** (65 mg, 0.1 mmol) was dissolved in 20 mL of ethanol in a Schlenk flask. The solution was purged with NO gas in the absence of oxygen, and the purple solution turned yellowish brown in less than 1 min. Thin plate-shaped crystals of **3** were formed upon standing overnight at 0 °C under a nitric oxide atmosphere. The crystals were collected by quickly filtering the solution under argon and briefly drying them under an argon stream with a slight vacuum. Loss of NO from the crystals and the regeneration of the starting material (**1**) were facile and clearly observable by the color change from brown to purple. Our inability to collect **3** as a dry solid without the loss of some NO prevented the acquisition of an acceptable elemental analysis. FT-IR (KBr): 1802 [ν(NO)], 1676 [ν(CO)], 1630, 1606 [ν_{as}(COO$^-$)], 1455 [ν_s(COO$^-$)], 1234, 1094 [ν_s(ClO$_4^-$)], 1008, 790, 756, 720, 680 cm^{-1}.

[Fe(TPA)(BF)(NO)](ClO$_4$) (4). Complex **2** (60 mg, 0.1 mmol) was dissolved in 20 mL of acetone in a Schlenk flask, and then exposed to NO gas; the solution turned brown in less than 1 min. Brown prismatic crystals of **4** suitable for X-ray crystallography were obtained by vapor diffusion of diethyl ether into the acetone solution at room temperature. Unlike those of **3**, crystals of **4** can be collected by filtering and drying under vacuum without loss of NO. Anal. Calcd for **4**·0.5(acetone), $C_{27.5}H_{26}ClFeN_5O_{8.5}$: C, 50.52; H, 4.01; N, 10.71; Cl, 5.42. Found: C, 50.79; H, 4.21; N, 10.45; Cl, 5.56. FT-IR (KBr): 1794 [ν(NO)], 1710, 1684 [ν(CO)], 1624, 1606 [ν_{as}(COO$^-$)], 1489, 1438 [ν_s(COO$^-$)], 1380, 1223, 1094 [ν_s(ClO$_4^-$)], 1022, 922, 780, 769, 719, 676, 624 cm^{-1}.

Crystallographic Studies of [Fe(TPA)(BF)(NO)](ClO$_4$)·0.5C$_3$H$_6$O (4). A brown prismatic crystal with approximate dimensions of 0.60

Table 2. Positional and Equivalent Isotropic Thermal Parameters for the Cation of [Fe(TPA)(BF)(NO)](ClO$_4$)·0.5C$_3$H$_6$O (**4**)

atom	x	y	z	B(eq),^{a} Å^2
Fe1A	0.6853	0.9094	0.7471	2.1(1)
O1wa	0.635(3)	0.909(1)	0.560(1)	6(1)
N1wa	0.658(2)	0.891(1)	0.634(1)	3.5(8)
O1A	0.632(2)	1.070(1)	0.7522(8)	2.4(5)
O2A	0.820(2)	1.164(1)	0.597(1)	4.3(7)
O3A	0.566(2)	1.229(1)	0.696(1)	4.2(7)
N1A	0.735(2)	0.925(1)	0.891(1)	2.0(3)
N11A	0.943(2)	0.983(1)	0.776(1)	2.0(3)
N21A	0.445(2)	0.832(1)	0.782(1)	2.9(3)
N31A	0.723(2)	0.740(1)	0.779(1)	1.9(3)
C1A	0.653(2)	1.159(2)	0.709(1)	2.4(4)
C2A	0.811(3)	1.197(2)	0.671(2)	3.8(5)
C11A	0.875(3)	1.031(2)	0.919(1)	2.6(4)
C12A	1.000(2)	1.039(2)	0.858(1)	2.6(4)
C13A	1.166(2)	1.094(2)	0.887(1)	2.4(4)
C14A	1.269(3)	1.095(2)	0.824(2)	3.9(5)
C15A	1.214(3)	1.044(2)	0.741(1)	3.4(5)
C16A	1.055(2)	0.986(2)	0.719(1)	2.9(4)
C21A	0.582(3)	0.937(2)	0.922(1)	3.4(4)
C22A	0.431(2)	0.854(2)	0.866(1)	2.5(4)
C23A	0.296(3)	0.802(2)	0.902(1)	3.1(4)
C24A	0.169(3)	0.729(2)	0.846(2)	4.6(5)
C25A	0.175(3)	0.706(2)	0.757(1)	3.6(4)
C26A	0.318(3)	0.759(2)	0.728(1)	2.9(4)
C31A	0.782(2)	0.820(2)	0.930(1)	2.4(4)
C32A	0.737(3)	0.714(2)	0.863(1)	3.1(4)
C33A	0.720(3)	0.602(2)	0.895(1)	3.4(4)
C34A	0.696(3)	0.518(2)	0.829(2)	4.2(5)
C35A	0.683(3)	0.532(2)	0.743(1)	3.6(4)
C36A	0.697(2)	0.648(2)	0.716(1)	2.7(4)
Fe1B	0.3166(4)	0.0888(3)	0.2548(2)	2.1(1)
O1WB	0.272(2)	0.215(1)	0.100(1)	5.1(8)
N1WB	0.317(2)	0.159(2)	0.155(1)	3.2(8)
O1B	0.155(2)	−0.072(1)	0.2177(8)	2.8(5)
O2B	−0.104(2)	−0.286(1)	0.127(1)	4.5(7)
O3B	0.142(2)	−0.070(1)	0.068(1)	4.7(7)
N1B	0.331(2)	0.022(1)	0.390(1)	2.4(3)
N11B	0.513(2)	0.001(1)	0.264(1)	2.1(3)
N21B	0.119(2)	0.146(1)	0.304(1)	2.4(3)
N31B	0.476(2)	0.238(1)	0.337(1)	2.0(3)
C1B	0.122(2)	−0.115(2)	0.139(1)	2.6(4)
C2B	0.048(3)	−0.250(2)	0.132(1)	2.4(4)
C11B	0.372(2)	−0.095(1)	0.383(1)	1.9(3)
C12B	0.511(2)	−0.078(2)	0.327(1)	2.3(4)
C13B	0.629(3)	−0.145(2)	0.341(1)	3.4(4)
C14B	0.737(3)	−0.133(2)	0.281(1)	3.1(4)
C15B	0.736(3)	−0.054(2)	0.217(1)	3.1(4)
C16B	0.628(3)	0.014(2)	0.210(1)	3.3(4)
C21B	0.154(2)	0.003(2)	0.411(1)	3.0(4)
C22B	0.084(2)	0.101(2)	0.378(1)	2.5(4)
C23B	−0.023(3)	0.142(2)	0.428(1)	3.4(4)
C24B	−0.092(3)	0.231(2)	0.391(1)	3.4(4)
C25B	−0.056(3)	0.271(2)	0.315(2)	4.8(6)
C26B	0.051(3)	0.227(2)	0.267(1)	3.4(4)
C31B	0.455(3)	0.104(2)	0.456(1)	3.2(5)
C32B	0.494(2)	0.226(2)	0.421(1)	2.2(4)
C33B	0.565(2)	0.323(2)	0.486(1)	2.7(4)
C34B	0.629(3)	0.432(2)	0.448(1)	4.3(5)
C35B	0.610(3)	0.442(2)	0.361(1)	3.9(5)
C36B	0.530(2)	0.343(2)	0.303(1)	2.3(4)

^{a} Anisotropically refined atoms are given in the form of the equivalent isotropic displacement parameter defined as $(4/3)[a^2\beta_{11} + b^2\beta_{22} + c^2\beta_{33} + ab(\cos\lambda)\beta_{12} + ac(\cos\beta)\beta_{13} + bc(\cos\alpha)\beta_{23}]$.

(15) Chiou, Y.-M.; Que, L., Jr. *J. Am. Chem. Soc.* **1992**, *114*, 7567−7568.
(16) Chiou, Y.-M.; Que, L., Jr. *J. Inorg. Biochem.* **1993**, *51*, 127.
(17) Chiou, Y.-M.; Que, L., Jr. *J. Am. Chem. Soc.* **1995**, *117*, 3999−4013.

Table 3. Selected Bond Lengths and Angles for Conformers **A** and **B** of [Fe(TPA)(BF)(NO)](ClO$_4$)·0.5C$_3$H$_6$O (**4**) and Related Structures[a]

a. Bond Lengths (Å)

	4A	4B	2	5
Fe1−N1w	1.70(2)	1.74(2)	2.137(6)[b]	1.790(5); 1.800(4)[c]
Fe1−O1	2.05(1)	2.05(1)	2.014(6)	2.038(6); 1.972(6)
Fe1−N1	2.16(2)	2.21(2)	2.220(7)	2.242(6); 2.198(7)
Fe1−N11	2.12(1)	2.16(2)	2.170(7)	2.133(6); 2.128(6)
Fe1−N21	2.16(2)	2.18(2)	2.218(7)	2.154(6); 2.199(6)
Fe1−N31	2.15(1)	2.15(1)	2.130(7)	2.105(6); 2.125(6)
N1w−O1w	1.15(2)	1.14(3)		
O1−C1	1.23(2)	1.26(2)		
O2−C2	1.21(3)	1.24(3)		
O3−C1	1.23(3)	1.22(3)		
C1−C2	1.51(3)	1.55(3)		
C2−C3	1.50(2)	1.47(3)		

b. Bond Angles and Torsion Angles (deg)

	4A	4B		4A	4B
N1w−Fe1−O1	97.3(7)	102.5(6)	N1w−Fe1−N1	175.5(8)	173.0(7)
N1w−Fe1−N11	100.7(8)	105.6(8)	N1w−Fe1−N21	104.8(7)	100.2(8)
N1w−Fe1−N31	97.8(7)	96.0(7)	O1−Fe1−N1	86.6(6)	84.3(5)
O1−Fe1−N11	93.2(5)	87.7(5)	O1−Fe1−N21	88.2(6)	88.8(6)
O1−Fe1−N31	163.7(5)	161.1(5)	N1−Fe1−N11	76.8(6)	76.2(6)
N1−Fe1−N21	77.4(6)	78.0(6)	N1−Fe1−N31	78.5(6)	77.1(5)
N11−Fe1−N21	154.1(6)	154.2(6)	N11−Fe1−N31	89.9(6)	91.2(6)
N21−Fe1−N31	82.2(6)	84.0(6)	Fe1−N1w−O1w	162(2)	155(2)
Fe1−O1−C1	137(1)	123(1)	O1−C1−O3	128(2)	131(2)
O1−C1−C2	118(2)	114(2)	O2−C2−C1	121(2)	118(2)
Fe1−O1−C1−O3	149(2)	−19(3)	O1−C1−C2−C3	−88(2)	−96(2)
Fe1−O1−C1−C2	−36(2)	160(1)	O1−C1−C2−O2	91(3)	86(2)

[a] Estimated standard deviations in the least significant figure are given in parentheses. [b] Fe−O(CH$_3$OH) bond distance (from ref 17). [c] Fe−μ-O bond distances (from ref 39).

× 0.25 × 0.25 mm was mounted on a glass fiber, coated with a viscous hydrocarbon, and quickly placed under a cold N_2 stream on the diffractometer. All data were collected on an Enraf-Nonius CAD-4 diffractometer with graphite-monochromated Mo Kα (λ = 0.710 69 Å) radiation. Cell constants and orientation matrixes for data collection were obtained from a least-squares refinement using the setting angles of 21 carefully centered reflections in the range 20.02 < 2θ < 39.30°. The data were collected using the ω scan technique to a maximum 2θ value of 48.4°. The intensities of three representative reflections which were measured after every 100 min of X-ray exposure time remained constant, indicating crystal stability. All data were corrected for empirical absorption and Lorentz−polarization effects.

The structure was solved by using Patterson and Fourier methods. The X-ray diffraction peaks for this crystal were broad, and there were a limited number of data. As a result, most of the atoms were treated as parts of groups or were left as isotropic, except for the iron, the nitrosyl, the BF oxygen atoms, and the chlorine atoms of the perchlorate anions, which were refined anisotropically. The rest of the non-hydrogen atoms were refined isotropically, and hydrogen atoms were placed in calculated positions (C−H = 0.95 Å). Refinement was carried out using a full-matrix least-squares routine on F with scattering factors and anomalous dispersion terms taken from a standard source.[18] The final cycle of full-matrix least-squares refinement was based on 2752 reflections ($I > 2.00\sigma(I)$) and 353 variable parameters. The maximum and minimum peaks on the final difference Fourier map corresponded to 0.66 and −0.70 e/Å^3, respectively. The structure is acentric; the entire unit cell contains two independent cations, two anions, and only one acetone solvate in the asymmetric unit. Some disorder in one of the ClO$_4$ groups was found during the refinement. Occupancies were fixed at 0.68 and 0.32 for two convergent groups to model this disorder. The structure was refined and converged to R = 0.084 and R_w = 0.076.

Some pertinent crystallographic details for **4**·0.5C$_3$H$_6$O are listed in Table 1. Fractional atomic coordinates for the complex are listed in Table 2, while selected bond distances and angles are collected in Table 3. The ORTEP plots of both conformers are shown in Figure 1. Further details, including ORTEP plots of both conformers with complete labeling schemes and tables of thermal factors, bond lengths, and bond angles, are provided in the supplementary material.

Physical Methods. Electronic spectra were obtained on a Hewlett Packard 8451A diode array spectrophotometer. ^{1}H NMR spectra of the complexes were obtained on a Varian VXR-300 or an IBM AC-300 spectrometer at 300 MHz and ambient temperature. Chemical shifts (in ppm) were referenced to the residual of protic solvent peaks. ^{1}H longitudinal relaxation times (T_1) were measured using the standard inversion-recovery pulse sequence (180°−τ−90°−AQ) with the carrier frequency set at several different positions to ensure the validity of the measurements. IR spectra of the complexes (KBr pellets) were obtained on a Perkin-Elmer FTIR 1600 series spectrometer. X-band EPR measurements were performed at liquid helium temperatures with a Varian E-109 spectrometer equipped with an Oxford cryostat. The magnetic field was calibrated with a gaussmeter, and the microwave frequency was measured with a counter.

Results and Discussion

Our interest in modeling the dioxygen-bound active sites of α-keto acid-dependent nonheme iron enzymes has led us to explore the coordination chemistry of nitric oxide with [Fe^{II}(L)(O$_2$CCOPh)]$^+$ complexes, where L is 6TLA or TPA (Chart 1). These efforts resulted in the preparation and characterization of two [Fe(L)(O$_2$CCOPh)(NO)]$^+$ complexes (**3** and **4**). The results are summarized in Scheme 1.

When NO (1 atm) was bubbled through an ethanol solution of **1** at room temperature in the absence of O_2, its characteristic purple-blue color converted almost instantaneously to yellowish brown. Allowing the solution to stand overnight at 0 °C under a nitric oxide atmosphere produced yellowish brown crystals. However, drying under vacuum or purging with argon regenerated the purple-blue color of **1**, indicating that NO was not tightly bound to the iron and could be easily removed. The binding of NO to **2** affording [Fe(TPA)(BF)(NO)](ClO$_4$) (**4**), on the other hand, was irreversible, and diffraction-quality crystals could be obtained by vapor diffusion of diethyl ether

(18) Cromer, D. T.; Waber, J. T. *International Tables for X-ray Crystallography*; Kynoch Press: Birmingham, England, 1974; Vol. IV.

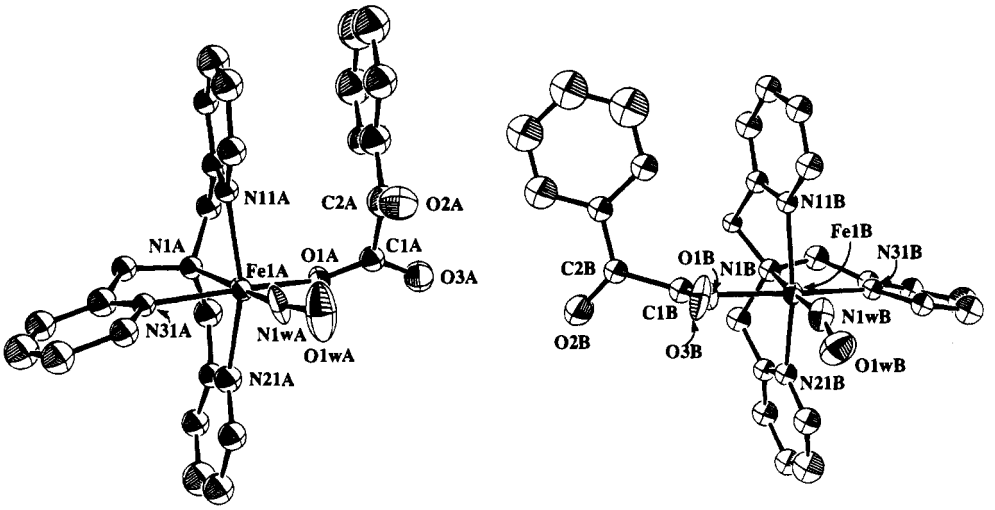

Figure 1. ORTEP view of two conformational isomers of $[Fe(TPA)(BF)(NO)]^+$ (**4**), showing 50% probability thermal ellipsoids. Hydrogen atoms are omitted for clarity.

Chart 1. Tripodal Ligands

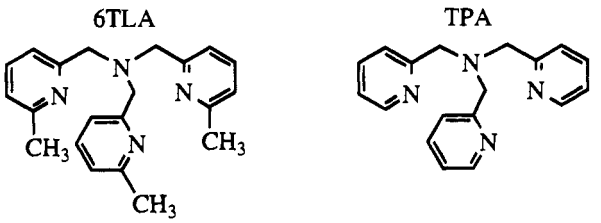

into an acetone solution of **4**. According to the formalism introduced by Enemark and Feltham,[19] both complexes **3** and **4** have an $\{FeNO\}^7$ configuration; i.e. the total number of electrons associated with the metal d orbitals and the NO π^* orbitals is *7*.

Description of the Structure of 4. X-ray diffraction studies show that **4** crystallizes in the triclinic system with space group *P*1 (No. 1). The structure is acentric with two independent $[Fe(TPA)(BF)(NO)](ClO_4)$ molecules (assigned as conformers **A** and **B**) and only one acetone molecule in the entire asymmetric unit cell. The two conformers are structurally equivalent, differing mainly in the orientation of the BF ligand (Figure 1). Both conformers contain a mononuclear, six-coordinate iron center coordinated to a tripodal tetradentate TPA ligand, a monodentate benzoylformate ligand, and a terminal bent nitrosyl. The geometry around the iron center is a distorted octahedron, as characterized by the angles N1w–Fe1–N11 of 100.7(8)° for **A** and 105.6(8)° for **B** and N1w–Fe1–N21 of 104.8(7)° for **A** and 100.2(8)° for **B**. A pseudomirror symmetry can be seen between the two conformers, except for the different orientations of their BF ligands, which give rise to Fe1–O1–C1–C2 torsion angles of −36(2)° for **A** and 160(1)° for **B**. The phenyl ring of benzoylformate is almost parallel with the N11A pyridine in conformer **A**, while its counterpart in **B** is tilted with respect to the N11B pyridine. Furthermore, the iron-bound NO is bent toward the BF ligand with an Fe–N–O angle of 162(2)° for conformer **A**, while the nitrosyl group is bent at 155(2)° toward the N21B pyridine in **B**.

Interestingly, the nitrosyl unit is trans to the tertiary amine (N1) of the TPA ligand and the BF ligand is trans to the N31 pyridine nitrogen in **4**; in contrast, in the structure of $[Fe^{II}(TPA)(BF)(MeOH)](ClO_4)$ (**2**), the BF ligand is trans to the amine nitrogen and the coordinated methanol is trans to one of the pyridine nitrogens.[17] This difference is best explained by the following trend in ligand strength:

$$NO > PhCOCOO^- > MeOH$$

For TPA and related complexes, the strongest ligand typically coordinates trans to the amine, which binds to the iron most weakly due to the constraints imposed by the coordination geometry of the tripodal ligand.[17,20–22] NO is an excellent π-acceptor and is capable of imparting unique stability to metal complexes by a synergistic interaction of σ-donation from NO onto the metal and π-back-donation of metal to the NO π^* antibonding orbitals.[23,24] Therefore, it is expected that NO should be trans to the tertiary amine nitrogen (a σ-only ligand), leaving the BF ligand to bind trans to a pyridine nitrogen. The closely related structure of $[Fe(TMPzA)(NO)Cl](BPh_4)$[25] also exhibits the same arrangement with the nitrosyl trans to the tertiary amine of the tripodal TMPzA ligand and the chloride trans to one of the pyrazoles.

As is typical for transition metal–nitrosyl complexes,[19,26,27] the coordinated NO in both conformers gives rise to short Fe–N and N–O distances (1.70(2) and 1.15(2) Å for **A** and 1.74(2) and 1.14(2) Å for **B**, respectively). The short Fe–NO distances indicate multiple-bond character between the iron and the nitrosyl ligand. The N–O bond lengths are comparable with the average value of 1.159 Å for a wide range of mononitrosyl complexes.[27] The Fe–N–O angles (162(2) and 155(2)°) are intermediate between the usual 180° linear and 120° "bent" metal nitrosyl extremes, and are slightly larger than the average

(19) Enemark, J. H.; Feltham, R. D. *Coord. Chem. Rev.* **1974**, *13*, 339–406.
(20) Holz, R. C.; Elgren, T. E.; Pearce, L. L.; Zhang, J. H.; O'Connor, C. J.; Que, L., Jr. *Inorg. Chem.* **1993**, *32*, 5844–5850.
(21) Ménage, S.; Zang, Y.; Hendrich, M. P.; Que, L., Jr. *J. Am. Chem. Soc.* **1992**, *114*, 7786–7792.
(22) Norman, R. E.; Holz, R. C.; Ménage, S.; O'Connor, C. J.; Zhang, J. H.; Que, J., L. *Inorg. Chem.* **1990**, *29*, 4629–4637.
(23) Richter-Addo, G. B.; Legzdins, P. *Metal Nitrosyls*; Oxford University Press: New York, 1992.
(24) Brown, C. A.; Pavlosky, M. A.; Westre, T. E.; Zhang, Y.; Hedman, B.; Hodgson, K. O.; Solomon, E. I. *J. Am. Chem. Soc.* **1995**, *117*, 715–732.
(25) Randall, C. R.; Zang, Y.; True, A. E.; Que, L., Jr.; Charnock, J. M.; Garner, C. D.; Fujishima, Y.; Schofield, C. J.; Baldwin, J. E. *Biochemistry* **1993**, *32*, 6664–6673.
(26) Mingos, D. M. P.; Sherman, D. J. *Adv. Inorg. Chem.* **1989**, *34*, 293–377.
(27) Feltham, R. D.; Enemark, J. H. *Top. Stereochem.* **1981**, *12*, 155–215.
(28) Pohl, K.; Wieghardt, K.; Nuber, B.; Weiss, J. *J. Chem. Soc., Dalton Trans.* **1987**, 187–192.

Scheme 1

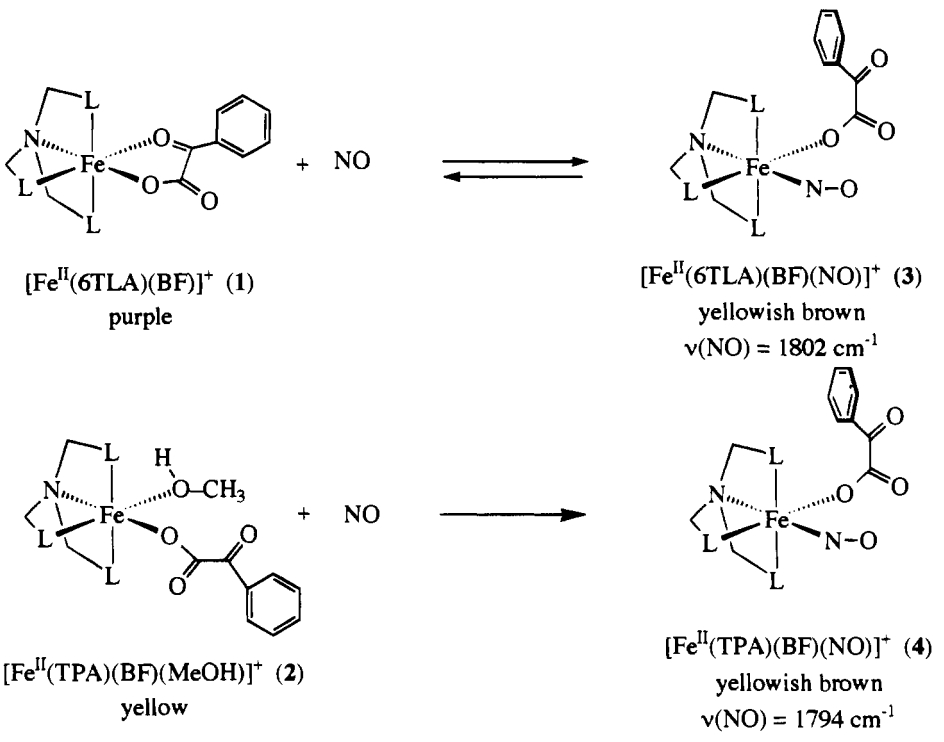

Table 4. Comparison of Synthetic Complexes with an $S = {}^3/_2$ {FeNO}7 Configuration

entry	complex	Fe–NO, Å	N–O, Å	Fe–N–O, deg	ν_{NO}, cm^{-1}	approx geometry and coordn no.	ref
1	[Fe(NO)(TPA)(BF)](ClO$_4$) (**4**)[a]	1.72(2)	1.15(2)	159(2)	1794	Oh, 6	this work
2	[Fe(NO)(Me$_3$TACN)(N$_3$)$_2$]	1.738(5)	1.142(7)	155.5(10)	1690	Oh, 6	28
3	[Fe(NO)(TMPzA)Cl](BPh$_4$)	1.725(7)	1.15(1)	157.1(8)	1796[b]	Oh, 6	25
4	[Fe(NO)(EDTA)]	1.78[c]	1.10[c]	156(5)[c]	1776	nd	24, 33
5	[Fe(NO)(salen)][d]	1.783(16)	1.10(3)	147(4)	1710	TP, 5	31
6	[Fe(NO)(TMC)(BF$_4$)$_2$][d]	1.737(6)	1.137(6)	177.5(5)	1840	TP, 5	32

[a] Bond lengths and bond angle are the average for both conformers. [b] Zang, Y.; Ming, L.-J.; Que, L., Jr. Unpublished results. [c] Determined by using GNXAS EXAFS analysis. [d] Measured at 23 °C. Both complexes exhibit a spin equilibrium: $S = {}^3/_2$ at room temperature and $S = {}^1/_2$ at low temperature (−175 °C).

bond angle of 146(11)° observed for $S = {}^1/_2$ {MNO}^{7} complexes.[27] Table 4 compares the properties of **4** with those of other high-spin {FeNO}^{7} complexes.[25,28–32] The three structurally characterized high-spin {FeNO}^{7} complexes are listed in entries 1–3, showing Fe–NO moieties with similar bond lengths and angles. [Fe(EDTA)(NO)] (entry 4) has a closely related Fe–N–O geometry as determined by GNXAS EXAFS analysis.[33] Entries 5[31] and 6,[32] on the other hand, are temperature-dependent spin-crossover systems and have rather different geometry and Fe–N–O angles. There are also numerous well-characterized five- and six-coordinate {FeNO}^{7} complexes, however, with a low-spin $S = {}^1/_2$ ground state.[34–38]

The remaining iron–ligand bond distances in **4** can be compared with those of other crystallographically characterized FeTPA complexes with carboxylate ligands, such as its precursor **2**[15,17] and the (μ-oxo)diiron(III) complex [Fe$_2$O(TPA)$_2$(O$_2$CCH$_3$)](ClO$_4$)$_3$ (**5**).[39] Complexes **2** and **4** represent the only pair of Fe(II)/FeNO complexes that have crystal structures. Complex **5**, on the other hand, represents a complex with iron(III) centers in a similar coordination environment, the short Fe–μ-oxo bonds being somewhat analogous to the even shorter Fe–NO bond in **4**. On the basis of the description of the Fe–NO unit as Fe(III)–NO$^-$,[24] a significant decrease in average bond length may be expected for **4** relative to that of its Fe(II) precursor **2**; such a shortening (0.1 Å) is observed in EXAFS studies of [Fe(EDTA)NO] relative to its precursor [Fe(EDTA)(H$_2$O)]$^-$.[33] However a comparison of the bond lengths found for **2**, **4**, and **5** (Table 3) does not substantiate this expectation. Indeed the average iron–ligand bond distances derived from

(29) Rich, P. R.; Salerno, J. C.; Leigh, J. S.; Bonner, W. D., Jr. *FEBS Lett.* **1978**, *93*, 323–326.
(30) Bonner, W. D., Jr.; Blum, H.; Rich, P. R.; Salerno, J. C. In *Frontiers of Biological Energetics*; Dutton, P. L., Leigh, J. S., Scarpa, A., Eds.; Academic Press: New York, 1978; Vol. 2; pp 997–1001.
(31) Haller, K. J.; Johnson, P. L.; Feltham, R. D.; Enemark, J. H.; Ferraro, J. R.; Basile, L. J. *Inorg. Chim. Acta* **1979**, *33*, 119–130.
(32) Hodges, K. D.; Wollmann, R. G.; Kessel, S. L.; Hendrickson, D. N.; Van Derveer, D. G.; Barefield, E. K. *J. Am. Chem. Soc.* **1979**, *101*, 906–917.
(33) Westre, T. E.; Di Cicco, A.; Filipponi, A.; Natoli, C. R.; Hedman, B.; Solomon, E. I.; Hodgson, K. O. *J. Am. Chem. Soc.* **1994**, *116*, 6757–6768.
(34) Enemark, J. H.; Feltham, R. D.; Huie, B. T.; Johnson, P. L.; Swedo, K. B. *J. Am. Chem. Soc.* **1977**, *99*, 3285–3292.
(35) Scheidt, W. R.; Frisse, M. E. *J. Am. Chem. Soc.* **1975**, *97*, 17–21.
(36) Scheidt, W. R.; Piciulo, P. L. *J. Am. Chem. Soc.* **1976**, *98*, 1913–1919.
(37) Scheidt, W. R.; Brinegar, A. C.; Ferro, E. B.; Kirner, J. F. *J. Am. Chem. Soc.* **1977**, *99*, 7315–7322.
(38) Karlin, K. D.; Rabinowitz, H. N.; Lewis, D. L.; Lippard, S. J. *Inorg. Chem.* **1977**, *16*, 3262–3267.
(39) Norman, R. E.; Yan, S.; Que, L., Jr.; Backes, G.; Ling, J.; Sanders-Loehr, J.; Zhang, J. H.; O'Connor, C. J. *J. Am. Chem. Soc.* **1990**, *112*, 1554–1562.

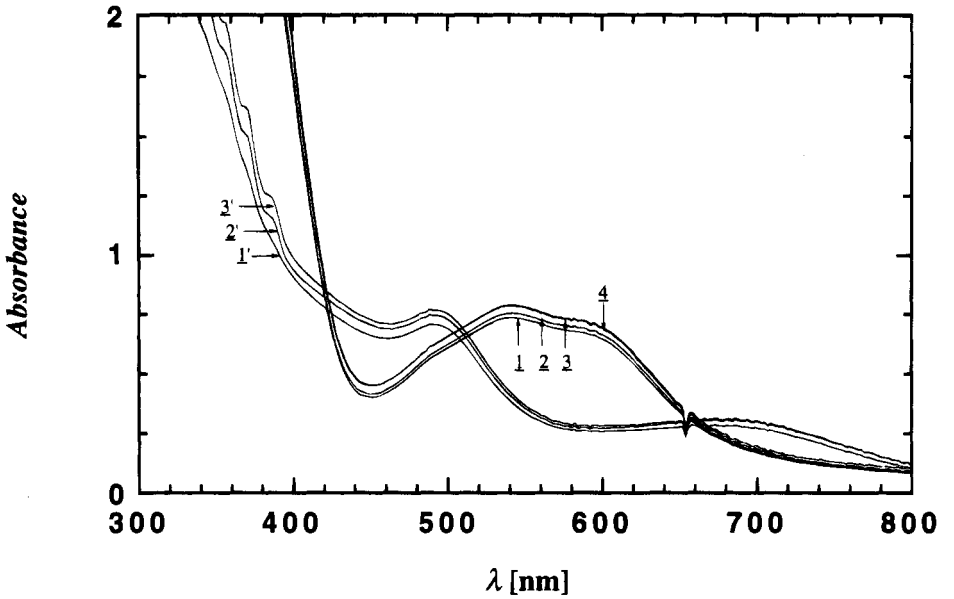

Figure 2. UV−vis spectra demonstrating the reversible NO binding behavior of [Fe(6TLA)(BF)](ClO$_4$) (**1**) in CH$_3$CN to give the NO adduct [Fe(6TLA)(BF)(NO)](ClO$_4$) (**3**) (*Ar/NO cycling*). Reaction of **1** (spectrum 1, λ_{max} at 544 nm and λ_{sh} at 590 nm) with NO at room temperature produces a yellowish brown solution of **3** (spectrum 1′, λ_{max} at 358, 372, 388, 492, and 690 nm). Purging of argon causes the regeneration of **1** (spectrum 2). The process can be repeated several times as shown with a small increase in absorbance due to the loss of solvent during the process.

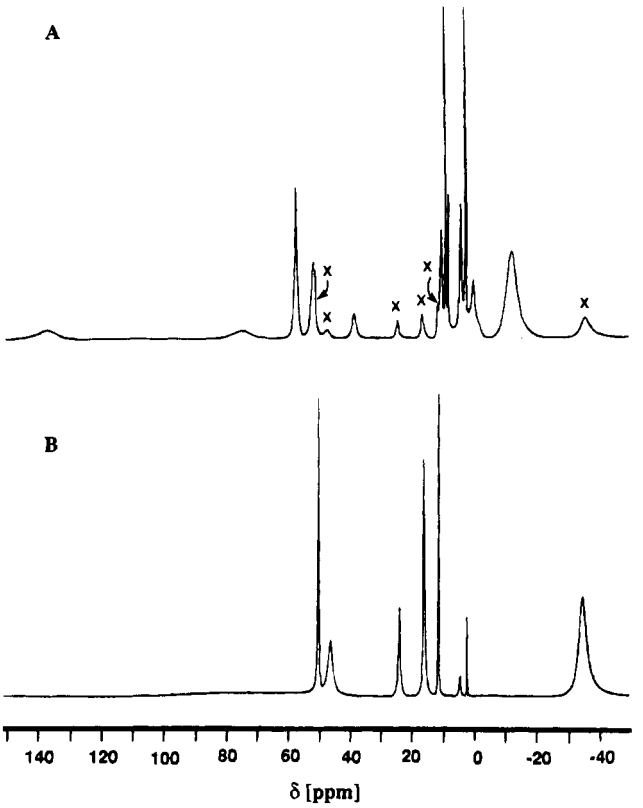

Figure 3. ^{1}H NMR spectra of [Fe(6TLA)(BF)(NO)](ClO$_4$) (**3**) (top), with peaks arising from **1** denoted by ×, [Fe(6TLA)(BF)](ClO$_4$) (**1**) (bottom) in CD$_3$CN.

the TPA ligand and the carboxylate for all three complexes differ only by 0.01 Å (2.15 Å for **2** and 2.14 Å for **4** and **5**). This comparison demonstrates that factors other than oxidation state affect metal−ligand bond lengths. While a decrease in metal−ligand bond lengths can be expected when Fe(II) is oxidized to Fe(III) due to the shrinking of its ionic radius, the presence of a strong metal−ligand interaction such as the Fe−NO or the Fe−μ-oxo bonds can counterbalance this effect and afford metal−ligand bond lengths that appear essentially unperturbed by the change in oxidation state.

Table 5. ^{1}H NMR Parameters[a,b]

assignt	1	2	3	4
CH_2	−[c]	53 (2.4)	136[e]	162 (0.20)[f]
			73[e]	142 (0.22)[f]
			38 (2.1)	124 (0.15)[f]
α-CH_3 or py α	−35 (0.60)	137 (1.1)	−12 (0.31)	105 (0.12)[f]
py β, β′	50 (7.3)	46 (8.4)	57 (6.6)	67 (3.2)
	46 (3.0)		51 (6.0)	61 (3.2)
				56 (3.2)
py γ	16 (~17)[d]	20 (22)	10.3 (~4.4)[d]	−2.3 (7.5)
BF *o*-H	24 (2.4)	9.0 (4.5)	10.0 (~2.4)[d]	10.6 (2.2)
m-H	11 (15)	8.6 (32)	8.6 (22)	8.6 (25)
p-H	16 (~17)[d]	8.2 (60)	7.7 (38)	7.7 (54)

[a] **1** = [Fe^{II}(6TLA)(BF)](ClO$_4$); **2** = [Fe^{II}(TPA)(BF)(ClO$_4$)]; **3** = [Fe(6TLA)(BF)(NO)](ClO$_4$); **4** = [Fe(TPA)(BF)(NO)](ClO$_4$). [b] Figures in parentheses are relaxation times (T_1) in milliseconds; in CD$_3$CN. [c] Too broad to be seen. [d] These two peaks are too close to measure separate relaxation times. [e] The relaxation time is too short to be measured. [f] CH_2 or py α protons of TPA ligand.

Physical Properties of the Nitrosyl Adducts. The purple color of [Fe^{II}(6TLA)(BF)](ClO$_4$) (**1**) turns yellowish brown immediately upon introduction of NO, indicating the formation of [Fe(6TLA)(BF)(NO)](ClO$_4$) (**3**). The UV−vis spectrum of **3** shows characteristic features at 358 (sh, ϵ 1900), 372 (sh, ϵ 1600), 388 (sh, ϵ 1200), 492 (ϵ 720), and 690 nm (ϵ 240 M^{-1} cm^{-1}). Bubbling argon through the NO solution for a few minutes or applying a vacuum restores the purple color of **1**. ^{1}H NMR analysis of the solution after NO is removed indicates a complete conversion back to the iron(II) starting material (complex **1**). Re-exposure to NO regenerates **3** (Figure 2). This process can be repeated several times without the decomposition of either compound, indicating reversible binding of NO to **1**.

The ^{1}H NMR spectrum of **1** in CD$_3$CN under NO clearly shows the presence of both **1** and **3** in solution (Figure 3). The equilibrium between the two complexes depends upon the quantity of NO in the solution; however, even under an NO atmosphere, a small amount (~16%) of complex **1** is present in solution, as determined by integration of the 6TLA α-CH_3 resonances. Table 5 lists the peak assignments for both complexes based on comparisons with other Fe(II)−TPA[21] and Fe(II)−6TLA[15] complexes and deductions from peak integration and relaxation time (T_1) measurements. Notice that the α-CH_3

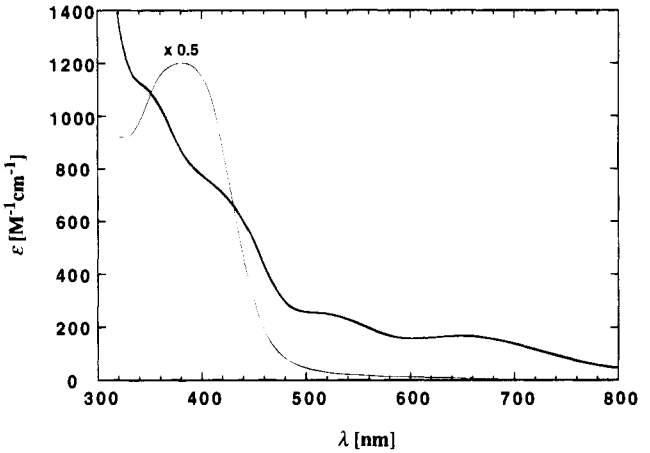

Figure 4. UV−vis spectra of [Fe(TPA)(BF)(NO)](ClO$_4$) (**4**) (bold line), featuring 350 (ϵ 1100), 420 (ϵ 730), 520 (ϵ 250), and 654 nm (ϵ 160 M^{-1} cm^{-1}), and [Fe^{II}(TPA)(BF)](ClO$_4$) (**2**) (plain line), with λ_{max} at 385 nm (ϵ 2400 M^{-1} cm^{-1}), in CH$_3$CN.

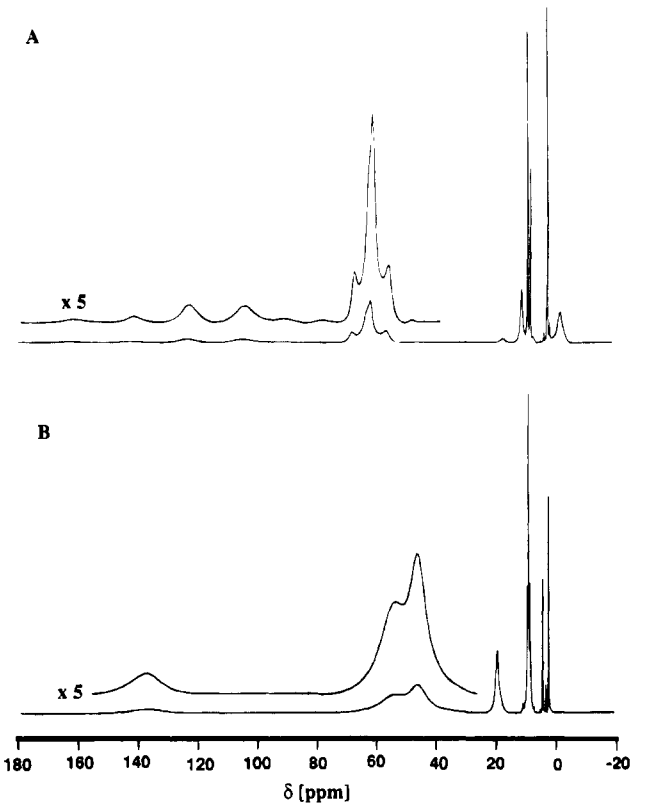

Figure 5. ^{1}H NMR spectra of [Fe(TPA)(BF)(NO)](ClO$_4$) (**4**) (top) and [Fe(TPA)(BF)](ClO$_4$) (**2**) (bottom) in CD$_3$CN.

groups of the 6TLA ligand were shifted from −35 to −12 ppm upon NO binding to the iron and, more dramatically, the BF protons were shifted from 24 (*o*-H), 11 (*m*-H), and 16 ppm (*p*-H) to 10, 8.6, and 7.7 ppm, respectively. The shifts and relatively small T_1 values of the BF protons in **3** indicate that the BF ligand remains coordinated to the iron center upon NO binding. From our earlier study of **1** and **2**,[15,17] the smaller chemical shifts of the BF protons in **3** indicate that NO has displaced the BF keto oxygen and the BF ligand is coordinated to the iron center only via its carboxylate oxygen. Therefore, the structure of **3** is proposed to be similar to that of **4** (Figure 1), with the nitrosyl group binding to the iron trans to the amine and cis to the monodentate BF ligand. From the number of peaks arising from the pyridine protons, the 6TLA ligand has an effective 3-fold symmetry in both **1** and **3**, indicating the

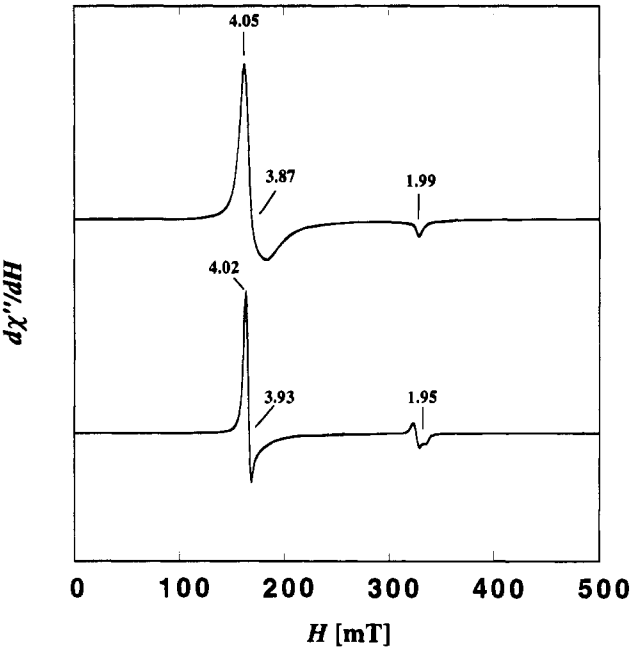

Figure 6. EPR spectra of frozen solutions of [Fe(TPA)(BF)(NO)](ClO$_4$) (**4**) (top) and [Fe(6TLA)(BF)(NO)](ClO$_4$) (**3**) (bottom). Samples are 2.0 mM in CH$_3$CN. The $g \approx 2$ region in the bottom spectrum arises from an anomalous signal of free NO in the solution. Instrumental conditions: microwave power, 0.02 mW; microwave frequency, 9.21 GHz; modulation frequency, 100 kHz; modulation amplitude, 1 mT; gain, 100; temperature, 4.0 K.

binding of NO to **1** is not only reversible but sufficiently facile as to average the pyridine environments on the NMR time scale.

On the other hand, treatment of [Fe^{II}(TPA)(BF)](ClO$_4$) (**2**) with NO results in the irreversible formation of [Fe(TPA)(BF)(NO)](ClO$_4$) (**4**), with features at 350 (ϵ 1100), 420 (ϵ 730), 520 (ϵ 250) and 654 nm (ϵ 160 M^{-1} cm^{-1}) (Figure 4). The ^{1}H NMR spectrum of **4** in CD$_3$CN (Figure 5A) displays features distinct from those of **2** (Figure 5B), and the absence of signals characteristic of complex **2** is consistent with a complete and irreversible formation of this nitrosyl complex. The relaxation times (T_1) of complex **4** are considerably shorter than those of **2**, indicating changes in the iron spin state. The peak assignments for **4** are also listed in Table 5. The BF protons essentially remain in the diamagnetic region with a slightly wider range of chemical shifts and shorter T_1 values than those of **2**. For **2**, the iron-bound solvent is labile in solution and the TPA ligand has effective 3-fold symmetry due to scrambling of its pendant pyridines along the Fe−N$_{amine}$ axis; the broad peaks observed for **2** may result from intermediate exchange (Figure 5B).[15,17] Upon binding of NO, the TPA ligand resonances lose their 3-fold symmetry, which is consistent with the irreversible binding of NO to complex **2**. It should be pointed out that, from the ^{1}H NMR spectral data of both iron−nitrosyl compounds (**3** and **4**), the BF ligand remains bound to the iron; thus the solid state structure shown in Figure 1 persists in solution in both cases.

NO coordination to the iron(II)−α-keto carboxylate complexes can also be demonstrated by infrared spectroscopy. The FT-IR spectra of **3** and **4** (KBr pellets) exhibit strong bands at 1802 and 1794 cm^{-1}, respectively. These bands are not observed in their parent complexes **1** and **2** and thus are assigned to the stretching frequencies of the coordinated NO, which are downshifted *ca.* 70−80 cm^{-1} from that of free NO (1875 cm^{-1})[23] due to the effect of the iron center. The 8 cm^{-1} difference in the NO stretching frequencies in **3** and **4** however is too small to infer differences in electronic structure that give rise to the differing NO binding affinities of **1** and **2**.

Table 6. Spectroscopic Parameters of Iron−Nitrosyl Adducts with an $S = {}^3/_2$ $\{FeNO\}^7$ Configuration

models/proteins	λ_{max}, nm (ϵ, M^{-1} cm^{-1})			*g* values	*E/D*	ref
[Fe(6TLA)(BF)(NO)](ClO4) (**3**)	358 (1900) 372 (1600) 388 (1200)	492 (720)	690 (240)	4.02, 3.93, 1.95	0.008	this work
[Fe(TPA)(BF)(NO)](ClO_4) (**4**)	350 (1100)	420 (730) 520 (250)	654 (160)	4.05, 3.87, 1.99	0.016	this work
[Fe(EDTA)(NO)]	340 (1300)	430 (900)	640 (200)	4.11, 3.95, 2.00	0.013	24, 33
IPNS−NO	340 (1800)	430 (800)	600 (200)	4.09, 3.95, 2.00	0.013	11
IPNS−ACV−NO		508 (1600)	720 (350)	4.22, 3.81, 1.99	0.035	11
2,3-CTD−NO	nr			4.18, 3.86, 1.99	0.029	13
				4.14, 3.90, 1.99	0.021	
				4.09, 3.97, 1.99	0.010	
2,3-CTD−cat−NO	nr			4.04, 3.98, 2.00	0.005	13
4,5-PCD−NO	nr			4.09, 3.90, 1.99	0.015	42
4,5-PCD−PCA−NO	nr			4.22, 3.77, 1.99	0.037	42
				4.37, 3.57, 1.99	0.064	
reduced 3,4-PCD−NO		430 (1870)	650 (sh, 400)	4.341, 3.693, 1.984	0.055	43
reduced 3,4-PCD−PCA−NO		404 (3930)	650 (400)	4.920, 2.988, 1.846	0.175	43
DeoxyHr−NO[a]		408 (1000)	500 (600)	2.76, 1.84		48, 49

[a] This is an $S_{eff} = {}^1/_2$ system, arising from the antiferromagnetic coupling between the $S = {}^3/_2$ $\{FeNO\}^7$ unit and the high-spin Fe(II) ($S = 2$) center.

The differing affinities of **1** and **2** for NO may be rationalized by examining their redox potentials. Complex **2** has an Fe^{III}/Fe^{II} redox potential of +340 mV vs NHE, and the potential for **1** is shifted to +870 mV due to the steric effects of the α-methyl groups of the 6TLA ligand.[17] The higher redox potential of **1** reflects the stability of the iron in its iron(II) state and explains the reversibility of NO binding, while **2** is more reducing and binds NO irreversibly. In studies of dioxygen binding to diiron(II) complexes, the introduction of 6-methyl groups to the pendant pyridines of $[Fe^{II}_2(HPTP)(OBz)]^{2+}$ converts an irreversible-dioxygen-binding complex to one that binds O_2 reversibly.[40,41]

Complexes **3** and **4** exhibit almost identical EPR spectra with intense resonances at $g = 4.02, 3.93, 1.95$ and $g = 4.05, 3.87, 1.99$, respectively (Figure 6). Both spectra are characteristic of a nearly axial $S = {}^3/_2$ spin state with *E/D* of 0.008 and 0.016 for **3** and **4**, respectively. Double integration of the EPR spectra shows that the EPR-active $S = {}^3/_2$ species accounts for ~80% of the iron in the sample of [Fe(6TLA)(BF)(NO)](ClO_4) (**3**) and >95% of the total spin in the sample of [Fe(TPA)(BF)(NO)](ClO_4) (**4**). The lower amount of **3** is consistent with the observation of reversible NO binding and the peak area integration results from the ^1H NMR study.

Relevance to the Biological Systems. The reaction of NO with catechol dioxygenases,[13,14,42,43] isopenicillin N synthase,[11,25] soybean lipoxygenase,[44,45] putidamonooxin,[46,47] and the reduced form of hemerythrin (deoxyHr)[48,49] has been exploited to great advantage to obtain electronic and structural information on the active sites of these proteins. As listed in Table 6, these nitrosyl complexes of native enzymes and enzyme−substrate complexes all exhibit axial $S = {}^3/_2$ EPR signals, with the exception of the deoxyHr−NO adduct, which has a dinuclear active site and shows a ground state $S_{eff} = {}^1/_2$ feature arising from antiferromagnetic coupling of the $S = 2$ iron(II) center and the $S = {}^3/_2$ $\{FeNO\}^7$ unit. They also exhibit similar UV−vis absorption with a characteristic three-band pattern in their UV−vis spectra (Table 6), with relatively intense absorption features in the near-UV region, followed by an absorption band with intermediate intensity in the 400−500 nm region and a weaker absorption band at 600−700 nm region, though the absolute band positions vary depending on the particular iron−nitrosyl complex (Table 6).

In order to make better use of these nitrosyl adducts as structural and spectroscopic probes, a detailed understanding of the electronic and geometric structure of the $\{FeNO\}^7$ system is required. The most straightforward strategy for obtaining such information is through the study of model complexes; however, synthetic compounds with an $S = {}^3/_2$ $\{FeNO\}^7$ configuration are not common in the literature. Our efforts to model the active site of α-keto acid-dependent enzymes have resulted in the characterization of two $[Fe(L)(NO)(O_2CCOPh)]^+$ complexes, which exhibit the $S = {}^3/_2$ $\{FeNO\}^7$ configuration and UV−vis absorption pattern characteristic of the nitrosyl adducts of many nonheme iron enzymes.

Complex **4**, $[Fe(Me_3TACN)(N_3)_2NO]$,[28] and [Fe(TMPzA)NOCl](BPh_4)[25] represent the only structurally characterized six-coordinate $\{FeNO\}^7$ complexes with an $S = {}^3/_2$ ground state; in addition the geometry of the Fe−NO unit in [Fe(EDTA)NO] has been determined by EXAFS with the use of the new data analysis package GNXAS.[33] A perusal of the information summarized in Table 6 shows that these four complexes exhibit very similar Fe−NO geometries with ∠Fe−N−O ~ 157°. On the basis of a detailed spectroscopic study of the TACN and EDTA complexes, Solomon *et al.* recently proposed that the $S = {}^3/_2$ $\{FeNO\}^7$ unit in these complexes is best described as a high-spin Fe(III) center ($S = 5/2$) antiferromagnetically coupled

(40) Dong, Y.; Ménage, S.; Brennan, B. A.; Elgren, T. E.; Jang, H. G.; Pearce, L. L.; Que, L., Jr. *J. Am. Chem. Soc.* **1993**, *115*, 1851−1859.
(41) Hayashi, Y.; Suzuki, M.; Uehara, A.; Mizutani, Y.; Kitagawa, T. *Chem. Lett.* **1992**, 91−94.
(42) Arciero, D. M.; Lipscomb, J. D.; Huynh, B. H.; Kent, T. A.; Münck, E. *J. Biol. Chem.* **1983**, *258*, 14981−14991.
(43) Orville, A. M.; Lipscomb, J. D. *J. Biol. Chem.* **1993**, *268*, 8596−8607.
(44) Salerno, J. C.; Siedow, J. N. *Biochim. Biophys. Acta* **1979**, *579*, 246−251.
(45) Nelson, M. J. *J. Biol. Chem.* **1987**, *262*, 12137−12142.
(46) Bernhardt, F.-H.; Gersonde, K.; Twilfer, H.; Wende, P.; Bill, E.; Trautwein, A. X.; Pfleger, K. In *Oxygenases and Oxygen Metabolism*; Nozaki, M., Yamamoto, S., Ishimura, Y., Coon, M. J., Ernster, L., Estabrook, R. W., Eds.; Academic Press: New York, 1982; pp 63−77.
(47) Twilfer, H.; Bernhardt, F.-H.; Gersonde, K. *Eur. J. Chem.* **1985**, *147*, 171−176.
(48) Nocek, J. M.; Kurtz, D. M., Jr.; Sage, J. T.; Debrunner, P. G.; Maroney, M. J.; Que, L., Jr. *J. Am. Chem. Soc.* **1985**, *107*, 3382−3384.
(49) Nocek, J. M.; Kurtz, D. M., Jr.; Sage, J. T.; Xia, Y.-M.; Debrunner, P.; Shiemke, A. K.; Sanders-Loehr, J.; Loehr, T. M. *Biochemistry* **1988**, *27*, 1014−1024.

to NO^- ($S = 1$) through direct orbital overlap.[24,50] The similarity of the spectroscopic properties of **3** and **4** to those of [Fe(EDTA)NO] suggests that a similar electronic description would also apply to these complexes. Such a description implies the transfer of an electron from iron(II) to NO upon binding and is analogous to that proposed for the binding of O_2 to the iron(II) center of the α-keto acid-dependent enzymes upon initiation of catalysis. The finding that structural features of $[Fe^{II}(L)(O_2CCOPh)]^+$ complexes modulate their NO binding affinity demonstrates that the ligand environment plays a role in binding NO and, by inference, O_2. Furthermore, the fact that $[Fe^{II}(L)(O_2CCOPh)]^+$ complexes can bind NO without losing their α-keto carboxylate ligand suggests that it is possible for the iron(II) center in these enzymes to have two or more sites occupied by cofactor and O_2 during the catalytic cycle. These compounds model a probable intermediate in the oxygenation reaction catalyzed by α-keto acid-dependent enzymes and will be useful benchmarks with which to compare the NO adducts of these enzymes, in the event such adducts become available. Furthermore, they can serve as models of the NO complexes of nonheme iron enzymes with carboxylate ligands such as isopenicillin N synthase,[25,51,52] lipoxygenase,[53,54] and extradiol-cleaving catechol dioxygenases.[55]

Acknowledgment. We are grateful to Professor Doyle Britton for his expertise in the X-ray diffraction experiments and to Professor John D. Lipscomb for the use of his EPR facility. Y.-M.C. thanks Dr. Timothy E. Elgren for suggesting this study. This work has been supported by the National Institutes of Health (Grant GM-33162).

Supplementary Material Available: For $[Fe(TPA)(BF)(NO)](ClO_4)\cdot 0.5$(acetone) (**4**), a crystallographic data table, ORTEP plots of conformers **A** and **B** with complete labeling schemes, and tables of positional coordinates, thermal parameters, bond lengths, and bond angles (26 pages). This material is contained in many libraries on microfiche, immediately follows this article in the microfilm version of the journal, and can be ordered from the ACS; see any current masthead page for ordering information.

IC9502638

(50) Zhang, Y.; Pavlosky, M. A.; Brown, C. A.; Westre, T. E.; Hedman, B.; Hodgson, K. O.; Solomon, E. I. *J. Am. Chem. Soc.* **1992**, *114*, 9189−9191.
(51) Ming, L.-J.; Que, L., Jr.; Kriauciunas, A.; Frolik, C. A.; Chen, V. J. *Inorg. Chem.* **1990**, *29*, 1111−1112.
(52) Ming, L.-J.; Que, L., Jr.; Kriauciunas, A.; Frolik, C. A.; Chen, V. J. *Biochemistry* **1991**, *30*, 11653−11659.
(53) Boyington, J. C.; Gaffney, B. J.; Amzel, L. M. *Science (Washington, D.C.)* **1993**, *260*, 1482−1486.
(54) Minor, W.; Steczko, J.; Bolin, J. T.; Otwinowski, Z.; Axelrod, B. *Biochemistry* **1993**, *32*, 6320−6323.
(55) Bolin, J. T.; Han, S.; Eltis, L. D. Results to be published.